A regional archeomagnetic model for Europe for the last 3000 years, SCHA.DIF.3K: Applications to archeomagnetic dating

F. Javier Pavón-Carrasco, Maria Luisa Osete, J. Miquel Torta, Luis R. Gaya-Piqué

Geochemistry Geophysics Geosystems G3
AN ELECTRONIC JOURNAL OF THE EARTH SCIENCES
Published by AGU and the Geochemical Society

Article
Volume 10, Number 3
25 March 2009
Q03013, doi:10.1029/2008GC002244
ISSN: 1525-2027

A regional archeomagnetic model for Europe for the last 3000 years, SCHA.DIF.3K: Applications to archeomagnetic dating

F. Javier Pavón-Carrasco and Maria Luisa Osete
Grupo de Paleomagnetismo, Departamento de Geofísica y Meteorología, Universidad Complutense de Madrid, E-28040 Madrid, Spain (fjpavon@fis.ucm.es; mlosete@fis.ucm.es)

J. Miquel Torta
Observatori de l'Ebre, CSIC, Universitat Ramon Llull, Horta Alta 38, E-43520 Roquetes, Spain (jmtorta@obsebre.es)

Luis R. Gaya-Piqué
Equipe de Géomagnétisme, Institut de Physique du Globe de Paris, CNRS, Tour 14, 2 place Jussieu, F-75005 Paris, France (gaya@ipgp.jussieu.fr)

[1] The available European database of archeomagnetic field values and instrumental data has been used to produce a regional model for the geomagnetic field in Europe for the last 3000 years (from 1000 B.C. to 1900 A.D., connecting with the epoch covered by the IGRF models). This new model, SCHA.DIF.3K, constitutes an improvement with respect to the previous regional archeomagnetic model SCHA.DI.00-F, which used relocated values and was only valid for the last 2000 years. The new model has been obtained by least sums of absolute deviation inversion of paleomagnetic data using spherical cap harmonics for the spatial representation of the field and sliding windows in time. An algorithm has been developed to jointly model the three archeomagnetic elements declination, inclination, and intensity. The resulting model provides the direction and intensity of the Earth's magnetic field over the European continent, northern Africa, and western Asia for the last 3000 years. The fit to the European archeomagnetic database is more accurate than that provided by global archeomagnetic models. In addition, this model represents a step forward in archeomagnetic dating studies (since the relocation error is avoided) and can also be used to study the rapid changes of the geomagnetic field (archeomagnetic jerks) that have been recently proposed.

Components: 11,416 words, 10 figures, 4 tables.

Keywords: Archaeomagnetism; geomagnetic secular variation; regional models; archaeomagnetic dating; archaeomagnetic jerks; Europe.

Index Terms: 1503 Geomagnetism and Paleomagnetism: Archeomagnetism; 1522 Geomagnetism and Paleomagnetism: Paleomagnetic secular variation; 1532 Geomagnetism and Paleomagnetism: Reference fields: regional, global.

Received 12 September 2008; **Revised** 15 January 2009; **Accepted** 6 February 2009; **Published** 25 March 2009.

Pavón-Carrasco, F. J., M. L. Osete, J. M. Torta, and L. R. Gaya-Piqué (2009), A regional archeomagnetic model for Europe for the last 3000 years, SCHA.DIF.3K: Applications to archeomagnetic dating, *Geochem. Geophys. Geosyst.*, *10*, Q03013, doi:10.1029/2008GC002244.

1. Introduction

[2] Paleosecular variation (PSV) describes the long-term temporal changes of the Earth's ancient magnetic field. The study of this variation improves our knowledge about the behavior of the magnetic field and the dynamics of the Earth's core.

[3] To define the geomagnetic field at any location three independent elements are needed. Several combinations are possible, but the measurements made most commonly in historical times were declination (D), inclination (I), and total intensity (F).

[4] Instrumental measurements of the directional (declination and inclination) Earth's magnetic field are available for the last few centuries, e.g., at London, 1570–1900 A.D. [*Malin and Bullard*, 1981]. Early historical measurements do not come from observatories, not even from single same locations, since permanent geomagnetic observatories were not established until the 19th century. These historical data sets are complemented by measurements of declination (mostly) and inclination for shipboard navigational purposes since the end of the 16th century [*Jackson et al.*, 2000; *Jonkers et al.*, 2003]. Instrumental intensity data are scarcer, the first measurements being taken in 1832 A.D. when Gauss invented a method for determining the absolute intensity values. For times prior to instrumental values, paleomagnetic data are needed. These data can be obtained from heated archeological structures (archeomagnetic data), from well-dated volcanic materials (lava flows), and from lake sediments which are well dated and undisturbed. Archeomagnetic data provide both directional and intensity data, whereas lake sediments contribute with directions and relative intensity only.

[5] Global models based on archeomagnetic data have been obtained during the last decade by using the Spherical Harmonic Analysis (SHA) technique, like the one proposed by *Hongre et al.* [1998], and the CALS family of models [*Korte and Constable*, 2003, 2005], which also includes lava flows and lake sediments as input data. These models represent the paleofield at a global scale, but they are usually too smooth to be used as a tool for archeomagnetic dating and to record rapid changes of the Earth's magnetic field (i.e., archeomagnetic jerks [*Gallet et al.*, 2003, 2005]).

[6] There are different reasons for the smoothness of the global models. For example in the model of *Hongre et al.* [1998] the smoothness is due to the small number of paleomagnetic data, and their inhomogeneous distribution around the globe. For the CALS models a trade-off was imposed between both spatial and temporal smoothness and fit to the global data, leading to a damping of variations also in regions and at times with dense data coverage. Very recently [*Lodge and Holme*, 2009], a test has been presented to demonstrate the feasibility of using the same regularized inversion strategy as in the CALS family to generate a viable regional dating tool. However, a definitive model still remains to be built.

[7] A possible solution to describe more accurately the long-term geomagnetic variations comes from the construction of Paleosecular Variation Curves (PSVC). These curves are the classical approach used by paleomagnetists to study the PSV in a region. To build a PSVC, a high density of well distributed in time paleomagnetic data from a small region (usually less than 600–900 km radius) are needed. The archeomagnetic data are then transferred from the sampling place to a reference point by the Conversion Via Pole method (CVP [*Noël and Batt*, 1990]). This relocation process introduces an error that, for the present geomagnetic field, increases with the relocation distance (a maximum of 7° for a 1700 km radius [*Casas and Incoronato*, 2007]).

[8] An intermediate approach between global models and PSVC is the determination of regional models. When analyzing the recent paleomagnetic compilations [e.g., *Korte et al.*, 2005] for the last 3000 years, it is observed that data are not homogeneously distributed around the globe, and the European continent is the region where the highest density of paleomagnetic data (mostly archeomagnetic data) is available: about 198 data/km^2 compared to 41 data/km^2 (Meso-America), 30 data/km^2 (North America), 23 data/km^2 (Asia), 3 data/km^2 (Oceania) and 1 data/km^2 (Africa) (values from *Korte et al.* [2005] and the updated European data set). *Korte et al.* [2005] show the temporal evolution of these data for each region or continent. Consequently a regional model at the European scale seems to be a realistic objective.

[9] In a recent paper, we proposed an initial regional model (the SCHA.DI.00 model [*Pavón-Carrasco et al.*, 2008a]) to describe the directional behavior of the paleomagnetic field in Europe for the last 2000 years, which was afterward updated by also modeling the paleointensity (the SCHA.DI.00-F model [*Pavón-Carrasco et al.*, 2008b]). The

SCHA.DI.00 and SCHA.DI.00-F models were developed using the spherical cap harmonic analysis technique (SCHA [*Haines*, 1985]) applied to directional data from five of the Bayesian European PSVC based on archeomagnetic data [*Pavón-Carrasco et al.*, 2008a, and references therein]. The intensity was added from the recent European paleointensity data set. These regional models seem to better reproduce the variability of the geomagnetic field over this region for the last 2000 years. However, the use of the PSVC as input data implied the inclusion of the relocation error into those models.

[10] In this paper, we propose a new regional archeomagnetic model for the European continent valid for the last 3000 years (1000 B.C. to 1900 A.D.): the SCHA.DIF.3K model (SCHA is the technique used to develop the model, D comes for declination, I for inclination, F for intensity, and 3K stands for the last 3000 years). Only archeological material has been used as input data because of the stability and origin of its remanence, commonly a thermoremanence (TRM) or a partial thermoremanence (pTRM) and because of the facility of some archeological materials to be accurately dated. Since the remanence acquisition mechanism for lake sediments is depositional (or postdepositional) a delay in the remanence acquisition time is expected. In addition, there seems to be some discrepancy in the determination of the paleointensity between the archeomagnetic and the lava flow records (M. Kovacheva, personal communication, 2008). For this reason we opted to use an internally consistent database, and therefore decided not to use any lake sediment and lava flow data in our study.

[11] The main differences between the SCHA.DIF.3K model and the initial SCHA.DI.00-F model [*Pavón-Carrasco et al.*, 2008b] are as follows:

[12] 1. For the input data, we have used the complete (with measurements up to 2007) "in situ" archeomagnetic data and three time series of historical observations of geomagnetic field directions, which we have denoted as "instrumental database." By using "in situ" data, the model is not affected by the relocation error. The instrumental database includes time series covering the last 4 centuries (from 1600 A.D. to 1900 A.D.) located in three western European countries (the United Kingdom, France and Italy).

[13] 2. The new model has been developed by jointly modeling the three archeomagnetic components (declination, inclination, and intensity). This model is more coherent than the previous regional models, for which in a first step the directional geomagnetic model was developed, and in a second step the intensity was added [see *Pavón-Carrasco et al.*, 2008a, 2008b].

[14] 3. The valid time period has been increased by 1000 years: from 1000 B.C. to 1900 A.D. (the SCHA.DI.00-F model was only valid from year 0 onward).

[15] The paper finishes with a demonstration of the main utility of the model as a tool for archeomagnetic dating and for the analysis of the rapid changes of the geomagnetic field (i.e., the so-called archeomagnetic jerks [*Gallet et al.*, 2003, 2005]) over the last three millennia.

2. Methodology

2.1. SCHA Technique

[16] The spherical cap harmonic analysis (SCHA) presented by *Haines* [1985] has been applied in many different studies [*Torta et al.*, 2006, and references therein]. The technique has been revised by *Thébault et al.* [2006] developing a new technique called revised spherical cap harmonic analysis (R-SCHA), for which a complete boundary value problem is solved. This method represents the magnetic field in a closed conical domain by a complete family of functions. The R-SCHA technique is an exact mathematical method, but the numerical problems are difficult to solve when only ground data are used. Very recently a new method (R-SCHA2D) for regional modeling of geomagnetic data over a spherical cap and at a constant altitude by using R-SCHA has been proposed [*Thébault*, 2008]. A further development of our work will be the study of the differences in the model results by using R-SCHA2D instead of SCHA.

[17] Some modelers prefer to use SHA with a regularized inversion strategy because of the following inherent limitations to SCHA: spatial structure limited by both the average minimum wavelength considered resolvable and by the shape of the limited number of basis functions, and difficulty to adapt the basis functions to irregular distributions of data within the cap. In regularized global inversions, the structure is constrained to minimize a specific measure of complexity in the field, and it is inherently adaptive to provide simple models in regions with few data. In our study, we

decided to follow the classical approach by *Haines* [1985], accepting the limitations of SCHA and the fact that the model cannot be extrapolated outside the limits of the cap. To model irregular distributions of data within the cap it is necessary to use a low maximum degree of the expansion. This low degree produces a spatial resolution for the regional archeomagnetic model that could be not too different from that of global models. On the other hand, the SCHA technique imposes an artificial conical boundary and it is not possible to study the power spectrum of the field and its behavior at the core-mantle boundary. In spite of these limitations, we think that a regional approach could better reproduce the variability of the geomagnetic field in Europe.

[18] The SCHA (and the R-SCHA) technique satisfies the Laplace equation and therefore we prefer to use this technique rather than other regional techniques (polynomial or spline modeling). The general solution that satisfies the conditions imposed by Laplace's equation is expressed for a spherical cap by an expansion in terms of spherical harmonics. The internal geomagnetic potential is:

$$V(r,\theta,\lambda) = a\sum_{k=0}^{K_{\text{int}}}\sum_{m=0}^{k}\left(\frac{a}{r}\right)^{n_k+1} P_{n_k}^{m}(\cos\theta) \cdot \left(g_{n_k}^{m}\cos m\lambda + h_{n_k}^{m}\sin m\lambda\right) \quad (1)$$

where P_{nk}^{m} (cos θ) are the colatitudinal Legendre functions, $(\frac{a}{r})^{n_k+1}$ is the radial dependence (with r the radial distance and a the mean radius of the Earth) and cos$m\lambda$, sin$m\lambda$ the longitudinal Fourier functions. g_k^m and h_k^m are the model's coefficients (SCH coefficients). The K_{int} parameter is the maximum degree of the expansion. The indices m and k are integers and the index $n_k(m)$ is real.

[19] In paleomagnetic studies, the elements usually determined for a given location are the declination, the inclination and the intensity. These components cannot be expressed by a linear combination of SCH coefficients. In the next section we will describe how we have solved this problem of linearization.

2.2. SCHA Applied to Directional and Intensity Data

[20] To express the archeomagnetic data as a linear function of the SCH coefficients, we have used the truncated Taylor's series applied to the expressions of the relationship between the declination, inclination and intensity and the Cartesian components of the geomagnetic field:

$$D = \arctan\left(\frac{Y}{X}\right)$$
$$I = \arctan\left(\frac{Z}{\sqrt{X^2+Y^2}}\right)$$
$$F = \sqrt{X^2+Y^2+Z^2} \quad (2)$$

[21] Expanding the series and taking into account equation (2), we obtain the general expression for the elements of the geomagnetic field:

$$\alpha(r,\theta,\lambda,t) = \alpha_0(r,\theta,\lambda,t) + \delta\alpha(r,\theta,\lambda,t) = \alpha_0(r,\theta,\lambda,t) + \left.\frac{\partial\alpha(r,\theta,\lambda,t)}{\partial g}\right|_{\alpha=\alpha_0}\cdot\delta g(t) \quad (3)$$

α (r, θ, λ, t) is the studied archeomagnetic element (declination, inclination or intensity), α_0 (r, θ, λ, t) is the initial value of the element given by a reference geomagnetic field. The variation of the element $\delta\alpha$ (r, θ, λ, t) is given by its derivative with respect to the SCH coefficients and their variation δg(t).

[22] The values of the derivatives of the archeomagnetic element by the SCH coefficients depend only on the initial reference field α_0 (X_0, Y_0 and Z_0):

$$\delta D = \frac{1}{H_0^2}\left(-Y_0\cdot\left(A_X^g, A_X^h\right) + X_0\cdot\left(A_Y^g, A_Y^h\right)\right)\cdot\delta g$$
$$\delta I = \frac{1}{F_0^2}\left(-\frac{Z_0X_0}{H_0}\left(A_X^g, A_X^h\right) - \frac{Z_0Y_0}{H_0}\left(A_Y^g, A_Y^h\right) + H_0\left(A_Z^g, A_Z^h\right)\right)\cdot\delta g$$
$$\delta F = \frac{1}{F_0}\left(X_0\left(A_X^g, A_X^h\right) + Y_0\left(A_Y^g, A_Y^h\right) + Z_0\left(A_Z^g, A_Z^h\right)\right)\cdot\delta g \quad (4)$$

where H_0 is the horizontal intensity and F_0 the total intensity of the reference geomagnetic field, and:

$$\left(A_X^g, A_X^h\right) = \sum_{k=0}^{K_{\text{int}}}\sum_{m=0}^{m=k}\left(\frac{a}{r}\right)^{n+2}\frac{dP_{n_k}^{k}(\cos\theta)}{d\theta}(\cos\lambda, \sin\lambda)$$
$$\left(A_Y^g, A_Y^h\right) = \sum_{k=0}^{K_{\text{int}}}\sum_{m=0}^{m=k}\left(\frac{a}{r}\right)^{n+2}\frac{m\cdot P_{n_k}^{k}(\cos\theta)}{\sin\theta}(\sin\lambda, -\cos\lambda)$$
$$\left(A_Z^g, A_Z^h\right) = \sum_{k=0}^{K_{\text{int}}}\sum_{m=0}^{m=k}\left(\frac{a}{r}\right)^{n+2}(n+1)P_{n_k}^{k}(\cos\theta)(-\cos\lambda, -\sin\lambda) \quad (5)$$

[23] There is an equation for every archeomagnetic data (declination, inclination or intensity) according to equations (4). These equations present spatial and temporal dependence.

[24] Before solving the problem, it is necessary to transform the coordinate system and the geomag-

netic elements to the SCHA reference frame. Two rotations are needed. First, we have transformed the coordinates and geomagnetic elements from geodetic (denoted by subscript gd) to geocentric (subscript gc). After this, we have rotated both coordinates and elements to the cap frame (subscript sch).

[25] For the first rotation, the geodetic longitude and the intensity are invariant; i.e., $\lambda_{gd} = \lambda_{gc}$ and $F_{gd} = F_{gc}$. To transform from geodetic to cap's coordinates the intensity changes along with radius but it is a small effect that cannot be taken account of by the SCH model since it needs data at uniform radius. To obtain the new geocentric colatitude (θ_{gc}), the radial distance (r_{gc}), the declination (D_{gc}) and the inclination (I_{gc}) one can easily adapt the subroutines given by *Haines* [1988]. It should be borne in mind that (1) for the pair declination-inclination, the transformation does not depend on the intensity value and (2) for single inclination values (without declination) we have associated a value to the declination equal to 0°. The maximum error made using this zero value for declination is very low (we have tested this error with synthetic data and it is lower than 0.02°).

[26] For the second rotation the radial distance, the inclination and the intensity are invariant ($r_{gc} = r_{sch}$, $I_{gc} = I_{sch}$ and $F_{gc} = F_{sch}$). The remaining coordinates (longitude λ_{sch} and colatitude θ_{sch}) and the declination (D_{sch}) can be transformed according to *De Santis et al.* [1989]:

$$\begin{aligned}\cos\theta_{sch} &= \cos\theta_0\cos\theta_{gc} + \sin\theta_0\sin\theta_{gc}\cos(\lambda_{gc}-\lambda_0)\\ \tan\lambda_{sch} &= \frac{-\sin\theta_{gc}\sin(\lambda_{gc}-\lambda_0)}{\sin\theta_0\cos\theta_{gc} - \cos\theta_0\sin\theta_{gc}\cos(\lambda_{gc}-\lambda_0)}\\ \tan D_{sch} &= \frac{\tan D_{gc} - \tan\alpha}{1+\tan D_{gc}\cdot\tan\alpha}\end{aligned} \tag{6}$$

where θ_0 and λ_0 are the cap's center coordinates and α is the angle between the north direction and the cap's center direction. This is given by:

$$\cos\alpha = \frac{\cos\theta_0 - \cos\theta_{gc}\cos\theta_{sch}}{\sin\theta_{gc}\sin\theta_{sch}} \tag{7}$$

2.3. Inversion Method

[27] To find the SCH coefficients that minimize the misfit we have to choose an appropriate inversion scheme. In a first attempt we used the classical iterative least squares (LS, L2 norm) inversion method. However, a detailed study of the error distribution showed that this distribution was not Gaussian but double exponential, so the use of the L2 norm was formally inappropriate. Therefore, and following the suggestion by an anonymous referee, we used the iterative least sums of absolute deviation (LAD, L1 norm) inversion. Differences between the L1 and L2 norms are related to the way the outliers are penalized. The L1 norm penalizes the outliers more than the L2 norm, so the residual data distribution is sharper. This type of distribution is called the Laplace (or double exponential) distribution.

[28] The LAD method is based in minimizing the absolute difference between real and modeled data. Taking into account the global data uncertainty (measurement uncertainty and time uncertainty) of the data (σ_i^{obs}), we have to minimize the function (χ_{L1}):

$$\chi_{L1}(t,a) = \sum_{i=1}^{n}\left\|\frac{x_i^{obs}(t,a) - x_i^{\mathrm{mod}}(t,a)}{\sigma_i^{obs}}\right\| \tag{8}$$

where t is the time, a is the location, $x_i^{obs}(t, a)$ is the real datum and $x_i^{mod}(t, a)$ is the modeled datum.

[29] For the inverse problem, we used an iterative approach. First we used an initial model as a reference model or input model (indicated by the subscript 0 in equation (4)) to obtain a new model by minimizing the equation (8). This new model will be used as the input model for a second iteration, and so on for successive iterations. The RMS error for each component of the geomagnetic field has been obtained taking into account the weight of the data $w_i^{obs} = 1/\sigma_i^{obs}$ (the weighting of the data is discussed in section 3.4):

$$rms = \sqrt{\frac{\sum_{i=1}^{n} w_i^{obs}\left(x_i^{obs} - x_i^{\mathrm{mod}}\right)^2}{\sum_{i=1}^{n} w_i^{obs}}} \tag{9}$$

[30] To solve the inverse problem for the temporal part, we have used a sliding windows technique, which is similar to the classical approach to construct paleosecular variation curves. The size of the window is related to the temporal data distribution and the age uncertainties. For each window, we have considered that each SCH coefficient ($g_i(t)$) can be defined by a cubic polynomial function, i.e., for the window i the SCH coefficients are given by:

$$g_i(t) = \sum_{p=0}^{3} g_{i,p}\cdot\left(\frac{t-t_0}{s}\right)^p \tag{10}$$

where t_0 is the central time of the window and s the size of the window. Thus, a spatial-temporal SCHA model was constructed for every s-year window. Finally, for every window we only took into account the $g_{i,0}$ parameter, so the resultant only spatial model is assumed valid for the center of the window (time t_0). This main $g_{i,0}$ coefficient is conditioned by all the remaining data into the window. The relation between two sets of consecutive SCH coefficients is smooth, because the windows are overlapping (in our case, we used a step of s/2). The size of the windows and the overlapping step conditioned the temporal resolution of the model. To evaluate how the sliding overlapping windows method affects the modeling results, we have carried out a test using synthetic data from the IGRF model at the same locations as those used in the archaeomagnetic database, and with similar dispersions and uncertainties. Results show that the variations (generated by the sliding windows method) are lower than the real variations given by the SCHA.DIF.3K model (especially for the inclination and intensity values). The temporal resolution, using the sliding windows method, is given by the time distance between 4 consecutive windows. In our case the window is overlapping s/2 years, so the temporal resolution is 3s/2.

3. Database and Input Data

3.1. Archeomagnetic Database

[31] We have used a recent data set of archeomagnetic data for Europe for the last 3000 years. The data set is based essentially on the database of *Korte et al.* [2005], (which consists of globally distributed paleomagnetic data). We have selected only the archeomagnetic data in the considered region (a cap of semiangle 40° center at 48°N and 9°E, i.e., Europe, north of Africa and west of Asia), excluding data from lava flows and sediments.

[32] From 2005 new data have been included in the database, largely because of the AARCH Network Project. These new data correspond to different European countries. For the directional data: Austria [*Schnepp and Lanos*, 2006], Germany [*Schnepp and Lanos*, 2005], Hungary [*Márton and Ferencz*, 2006], France [*Chauvin et al.*, 2000], Italy [*Evans and Hoye*, 2005; *Tema et al.*, 2006], Spain [*Gómez-Paccard et al.*, 2006a; *Ruíz-Martínez et al.*, 2008; G. Catanzariti, personal communication, 2008] and Greece [*Evans*, 2006]. And for the intensity: France [*Gallet et al.*, 2005] and Spain [*Gómez-Paccard et al.*, 2006c]. The initial number of the directional paleomagnetic data considered is 1464 for declination and 2018 for inclination. Intensity data also come from archeomagnetic artifacts. The initial number of archaeointensity data is 927.

[33] We have applied a filter based on the statistical uncertainty of directional paleomagnetic data. The precision of directional data is given by the parameter $\alpha_{95}{}^{\circ}$ (value for the 95% confidence cone about the mean direction). The intensity data has precision given by the parameter σ_F. We have rejected all data whose α_{95° is three times bigger than the mean α_{95°. A similar criterion has been applied to intensity data (three times the mean σ_F). After applying this filter, we have rejected 26 directional data (1 from Poland, 6 from Russia, 5 from Ukraine, 10 from United Kingdom, 2 from Germany, and 2 from Italy) and 12 intensity data (3 from Slovakia, 1 from France, 1 from Serbia, 3 from Egypt, 3 from United Kingdom, and 1 from Russia). The mean values of α_{95° and σ_F are 4.1° and 3.3 μT, respectively. We have also rejected those data with age uncertainties greater than 500 years (9 data from United Kingdom and 3 from Hungary).

[34] The definitive archeomagnetic database consists of 1437 declination data, 1979 inclination data and 913 intensity data.

3.2. Distribution of Archeomagnetic Input Data

[35] Figure 1 shows the spatial distribution of the archeomagnetic data (declination, inclination and intensity) used as input data for the time interval 1000 B.C. to 1900 A.D. The distribution of data in Europe is inhomogeneous, so in order to visualize the number of data in every region we have represented the spatial distribution of the data according to the latitude and longitude coordinates relative to the cap's center: 48°N latitude and 9°E longitude (orange lines in Figure 1).

[36] The colatitudinal distribution (Figure 2a) of declination and inclination are similar. Both show that the data are distributed inside a cap with semiangle 22° (except for some inclination data, up to 25° away from the cap center). A higher data density is found between 3° and 15° of colatitude, marked with high peaks between 5° and 10°. The inclination registers two other maxima in the number of data at about 11° and 19° of colatitude (corresponding to Bulgarian and eastern European data respectively). Intensity data are concentrated between 11° and 15° of colatitude. There is a second smaller concentration peak around 7°

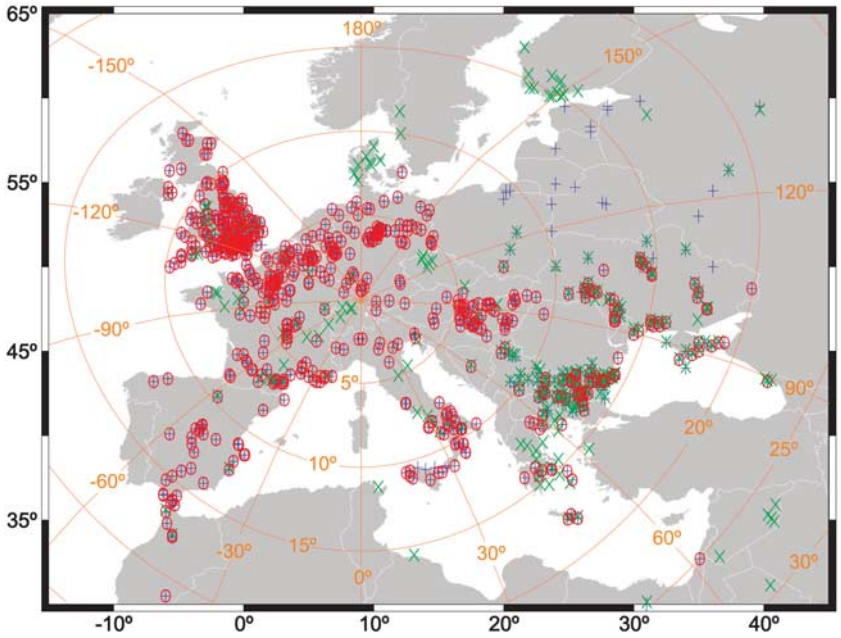

Figure 1. Locations of input data. Declination (red circles), inclination (blue pluses), and intensity (green crosses). Orange grid shows colatitude and longitude relative to the cap's center (48°N, 9°E).

corresponding to Hungarian data. The furthest data are about 28° away from the center of the cap (Middle East).

[37] Figure 2b shows the longitudinal distribution of the data. Again, both declination and inclination distributions are similar. The western European data (negative longitudes) are almost identical, so it is obvious that declination data have inclination data associated. For positive longitudes, i.e., eastern Europe, the number of inclination data is higher than declination data. France and the United Kingdom (about −125° longitude) in the western part of the cap, and Bulgaria and Hungary (between 60° to 90° of longitude) in the eastern part have the highest concentration of archeomagnetic directional data.

[38] The spatial distribution of the intensity data of Figure 2b is very significant since it shows the elevated difference between the number of intensity data from western and eastern Europe. From the 927 initial intensity data, only 139 data are from western countries. This may have consequences for the development of the regional model, because the east intensity data are predominant over the rest of the intensity data. The highest concentration of intensity data are in Greece (50° longitude), Bulgaria (about 70° longitude), and Hungary (90° longitude).

[39] The temporal distribution of data (Figure 2c) shows a high density in the Roman period (between 100 B.C. and 500 A.D.) and between the 9th and 19th centuries A.D. There is a decrease in the density of data for 500–1000 A.D. (the so-called "Dark Ages"). There are more intensity data than directional data before 100 B.C.

[40] In the time interval 1000 B.C. to 1900 A.D., the declination ranges in Europe between −33.7° and 42.9° with an average uncertainty of 4.6° and a standard deviation of 2.5°. Inclination varies between 32.5° and 86.0°, with a mean uncertainty of 2.3° and a standard deviation of 1.1°. The upper and lower limits of intensity are 33.0 μT and 101.0 μT, with 3.4 μT and 2.0 μT of mean uncertainty and standard deviation respectively. The mean age uncertainty for all data is 53.0 years with a standard deviation of 67.0 years. All data uncertainties are given at 68% of confidence.

3.3. Instrumental Data

[41] We have included three historical time series of the direction of the Earth's magnetic field for the last 400 years (∼1600–1900 A.D.) located at London, Paris and many Italian localities (Figure 3). The first series is given by the compilation of *Malin and Bullard* [1981], which reports the direction of the Earth's magnetic field at London from 1570 to

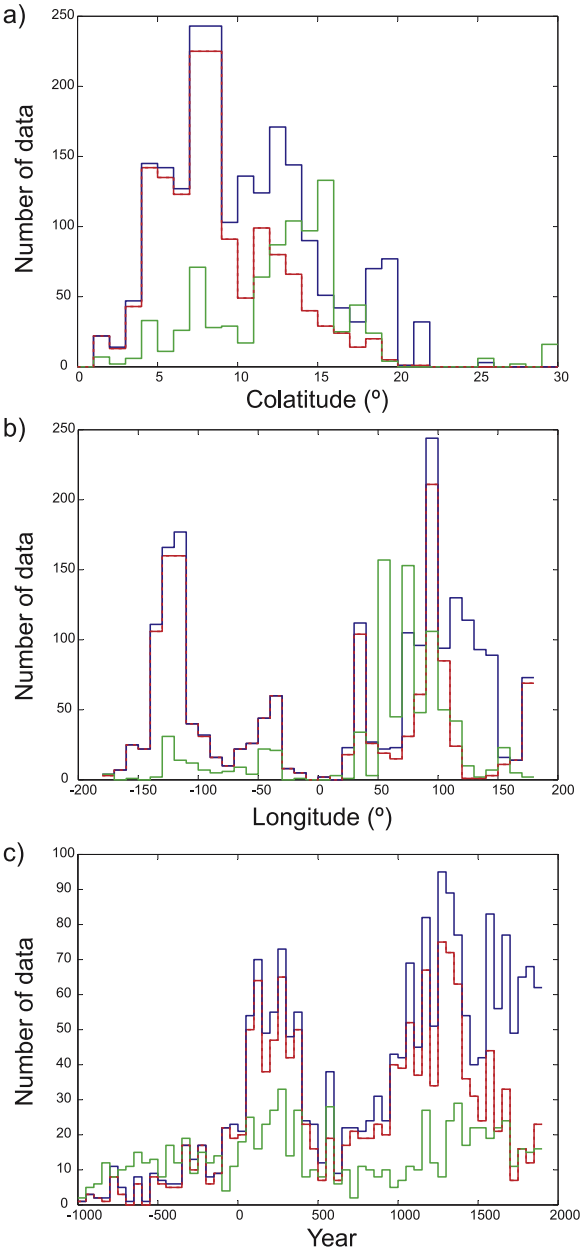

Figure 2. Histograms of declination (red), inclination (blue), and intensity (green) data through (a) colatitude, (b) longitude, and (c) time. Both colatitude and longitude are referred to the cap's center (orange grid in Figure 1). The size of the bins are 1° for colatitude, 10° for longitude, and 50 years for time.

1975 A.D. *Alexandrescu et al.* [1996] compiled the instrumental series of the geomagnetic field direction in Paris (from ~1550 to 1994 A.D.). Finally, the instrumental series from Italy includes historical measurements at many localities since 1640 [*Cafarella et al.*, 1992, and references therein], complemented by the records of the Pola observatory (north of Italy, nowadays in Croatia, from 1881 to 1909 A.D.).

[42] We have assigned a constant value to the uncertainties of the instrumental series. The observatory directional data used have not been corrected for crustal anomalies and they may present an error related to correlation. According to this reason the use of original uncertainties is not appropriate. *Jackson et al.* [2000] indicated that the use of different observation sites can generate about 0.5° noise in the observations, so in order to solve this problem we have assigned a constant uncertainty of 0.5° for all declination and inclination instrumental data.

[43] We have not used instrumental intensity data because they start progressively from 1832 A.D. onward, while our model has an upper limit at 1900 A.D.

[44] Figure 3 shows all instrumental series, which have been reduced (we have used the relocated data as given in the original works) to three reference points (London coordinates for the first series: 51.5°N latitude and 0.1°W longitude), Paris (48.1°N, 2.3°E) for the second and Viterbo (42.5°N, 12.0°E) for the Italian series). They are

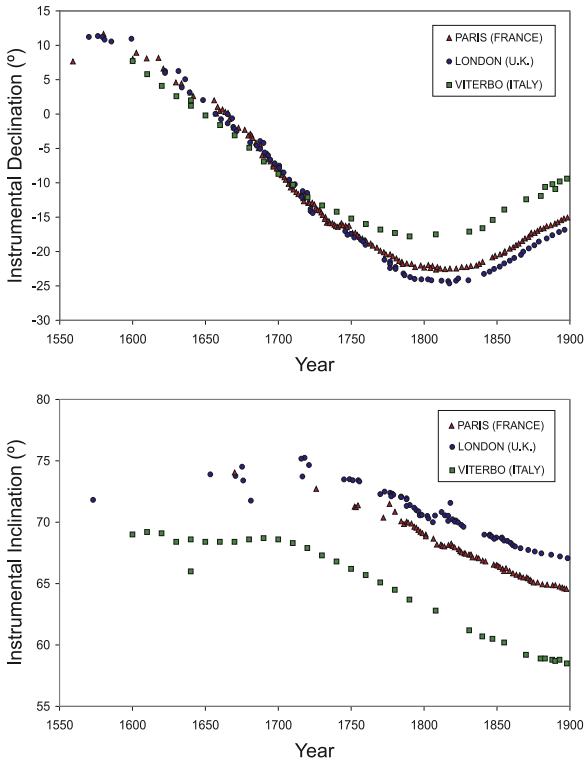

Figure 3. Series of directional instrumental data. All data have been reduced to the reference point (see legend).

in general annual mean values. We have analyzed the relocation error for the three time series: The directional Italian data set comes from many locations distributed all over the country. Using the synthetic data from the GUFM model [*Jackson et al.*, 2000] we have calculated the relocation error for all time interval (1600–1900 A.D.); this error is lower than 0.2° for the declination and 0.1° for the inclination. The French and English data sets are distributed very near to the reference location. We have also calculated the relocation error using GUFM model for the corresponding time interval. These errors are close to zero (0.07° and 0.03° for declination and inclination respectively).

3.4. Weighting of the Data

[45] We have added an additional uncertainty (τ_i) to the measurement uncertainty (ρ_i) depending on the age uncertainty value, applying the same criteria as in the work by *Korte et al.* [2005] but modified because of the use of sliding windows; the final uncertainty is therefore the square root of the sum of the squares of the measurement uncertainty (ρ_i) and the uncertainty associated to age (τ_i). The value of τ_i for each datum has been normalized according to the following scheme. Each datum is given by a mean age t_0 and an age uncertainty t_m, so it spreads over the whole time interval: $[t_0 - t_m, t_0 + t_m]$. To take this into account in the model, we normalized the uncertainty by introducing a factor depending on the location of the datum inside the temporal window. There are 4 possible cases for a window limited by $[t_1, t_2]$.

[46] 1. The datum is completely within the time window: $t_1 < t_0 - t_m$ and $t_0 + t_m < t_2$. In this case the normalization factor is 1. The datum mean age is given by t_0.

[47] 2. Part of the datum is within the window. There are two types: (1) If $t_0 - t_m < t_1$ and $t_0 + t_m < t_2$, the normalization factor is given by $f = 2 \cdot t_m/(t_0 + t_m - t_1)$, and the datum mean age is $(t_0 + t_m + t_1)/2$. (2) If $t_1 < t_0 - t_m$ and $t_0 + t_m > t_2$, the normalization factor is given by $f = 2 \cdot t_m/(t_2 - t_0 + t_m)$, and the mean age is $(t_2 + t_0 - t_m)/2$.

[48] 3. Finally, if $t_0 - t_m < t_1$ and $t_2 < t_0 + t_m$, the normalization factor is $f = 2 \cdot t_m/(t_2 - t_1)$, and the datum mean age is given by the mean time of the window, $(t_1 + t_2)/2$.

[49] Therefore, the final uncertainty (σ_i) is given by:

$$\sigma_i = f \cdot \left(\rho_i^2 + \tau_i^2\right)^{1/2} \tag{11}$$

and the weight of the datum is given by the inverse of the uncertainty:

$$w_i = \frac{1}{\sigma_i} = \frac{1}{f} \cdot \left(\rho_i^2 + \tau_i^2\right)^{-1/2} \tag{12}$$

4. Model Parameters and Result: SCHA.DIF.3K Model

4.1. Model Parameters

[50] Previous studies have shown that, in order to produce a spatial-temporal model from archeomagnetic data using SCHA it is necessary to consider relatively large size caps and a low degree spherical harmonic expansion [*Pavón-Carrasco et al.*, 2008a]. In this new study we keep the same maximum spherical cap harmonic index that was used for the initial model built from the European PSVC [*Pavón-Carrasco et al.*, 2008a], i.e., K = 2. Given the size of the spherical cap used ($\theta_0 = 40°$) and the maximum data resolution, the model represents the same spatial wavelength as a global (SHA) model with maximum degree n = 5.

[51] Taking into account the spatial distribution of data, the cap has been situated centered on Austria, at 48°N latitude and 9°E longitude (see Figure 1). The temporal distribution of data and the associated age uncertainty have conditioned the size of the windows for the temporal expression of the inverse problem. The optimal size of the window is 50 years, because the mean age uncertainty is 53 years. Within each window there are, on average, 29 declination data, 38 inclination data, and 15 intensity data (see Figure 2c), except for two windows which have no declination values (750 B.C. to 700 B.C., and 650 B.C. to 600 B.C.).

[52] For each time window we have applied a spatial-time fitting by the iterative LAD technique using equations (8) and (10). By moving the window at 25 years steps from 1000 B.C. to 1900 A.D., we obtain 117 sets of SCH coefficients.

4.2. Input Models

[53] To obtain the new regional model, we have used two initial reference models (these models are only used in the first iteration) for two time intervals: the SCHA.DI.1-F from 1000 B.C. to 1650 A.D., and the GUFM model [*Jackson et al.*, 2000] from 1650 to 1900 A.D.

[54] The SCHA.DI.1-F is an extension of the SCHA.DI.00-F, since the previous has a temporal

Table 1. Number of Initial and Rejected Data

Component	Initial Number of Data	Rejection Criterion	Number of Rejected Data	% of Rejected Data
Declination	1437	$\sigma_D > 3 \cdot 4.9°$	89	6.2%
Inclination	1979	$\sigma_I > 3 \cdot 2.9°$	114	5.8%
Intensity	913	$\sigma_F > 3 \cdot 6.6\ \mu T$	24	2.6%

validity from 0 to 1900 A.D. To build the new model, SCHA.DI.1-F, valid from 1000 B.C. up to 1900 A.D., we have used the European PSVC from 1000 B.C. to 0 (France [*Gallet et al.*, 2002], Germany [*Schnepp and Lanos*, 2005], Hungary [*Márton and Ferencz*, 2006], Iberia [*Gómez-Paccard et al.*, 2006b], and the United Kingdom [*Zananiri et al.*, 2007]) and applied the same procedure described by *Pavón-Carrasco et al.* [2008a, 2008b].

[55] From 1650 A.D. onward we used the GUFM model because this model appears to be the most suitable one after the 17th century. The model has been modified with a new value for the first Gauss coefficient g_1^0 from 1590 A.D. to 1840 A.D. given by *Gubbins et al.* [2006]; the modification thus applies only to the prediction of the intensity before 1840 A.D.

[56] The change in initial reference models was chosen at 1650 A.D. because the minimum difference between both models occurs at this epoch [*Pavón-Carrasco et al.*, 2008a, 2008b]. To estimate the difference between the SCHA.DI.1-F and the modified GUFM model at 1650 A.D. we have calculated the difference between predicted data from both models at the location of the input data from 1625 A.D. to 1675 A.D. Declination shows the most abrupt change, the main difference being 4.7° with a deviation of 3.2°. The differences for inclination and intensity are more reasonable: $1.9° \pm 1.0°$ and $2.2\ \mu T \pm 1.5\ \mu T$, respectively. Despite these differences, the final SCHA.DIF.3K model shows a smooth behavior in the time period from 1600 A.D. to 1700 A.D. The reason is that the difference between SCHA.DI.1-F and modified GUFM models at 1650 A.D. is smaller than the uncertainties of the archeomagnetic data in the window 1625–1675 A.D.

[57] To evaluate how the input model affects the final model, we performed tests using the following three archaeomagnetic models: (1) CALS7K.2 model, (2) SCHA.DI.1-F model, and (3) a simple dipolar model. This dipolar model was obtained from the relocation of all the data at the cap's center and calculating the average Fisher direction and the average intensity (in the same way as a palaeosecular curve is generated).

[58] The study showed that for temporal windows with a high data density, the final model was similar for all three cases. However, for windows with a low density of data (for B.C. windows), the input model determined the final model. For this reason, we decided to use the most suitable model according to the updated input data, i.e., the regional archaeomagnetic model SCHA.DI.1-F.

4.3. SCHA.DIF.3K Model

[59] The SCHA.DIF.3K has been obtained following an iterative procedure in which outliers are rejected. A first SCHA model is obtained and used to remove those data with residuals greater than 3 times the average value of RMS misfit error. Table 1 shows the number of rejected data. No data from historical series have been rejected.

[60] With the selected database, the regional SCHA.DIF.3K model has been finally obtained after an average of 6 iterations per window. Table 2 shows the initial and final RMS misfits for every temporal window and the number of iterations. The optimal model is given by the iteration not varying the RMS misfit by more than 1% of its value.

[61] To obtain the model uncertainty (at 95% of confidence) of the predicted values for the regional model, we have used a spatial function, $C(t, \varphi, \lambda)$, for every element, i.e., declination, inclination and intensity. This function is obtained by the spatial-time distribution of the RMS misfits for each window by using a gridding method (polynomial in space and time). The $C(t, \varphi, \lambda)$ function defines the prediction uncertainty for the three components of the Earth's magnetic field at any location and time (at 95% of confidence). Figure 4 shows the $C(t, \varphi, \lambda)$ function for different locations in the valid time period.

Table 2. Initial and Final RMS Misfits and Number of Iterations for Every Temporal Window[a]

t_0	Number of Iterations	Initial RMS	Final RMS
−975	5	0.81	0.50
−950	5	0.63	0.41
−925	5	0.58	0.39
−900	6	0.67	0.48
−875	6	0.65	0.49
−850	5	0.67	0.50
−825	6	0.73	0.60
−800	7	0.76	0.65
−775	6	0.71	0.60
−750	6	0.79	0.67
−725	8	0.79	0.64
−700	9	0.90	0.71
−675	7	0.97	0.82
−650	7	0.87	0.71
−625	7	0.89	0.73
−600	6	0.90	0.80
−575	6	0.81	0.70
−550	8	0.90	0.76
−525	6	0.82	0.71
−500	7	0.86	0.72
−475	9	0.86	0.70
−450	9	0.99	0.81
−425	6	0.98	0.87
−400	9	1.20	1.06
−375	7	1.13	1.03
−350	7	1.18	1.05
−325	6	1.19	1.09
−300	5	1.16	1.06
−275	5	1.09	1.01
−250	5	1.05	0.95
−225	7	0.93	0.81
−200	8	0.53	0.41
−175	7	0.85	0.71
−150	7	0.94	0.72
−125	4	0.93	0.83
−100	11	0.85	0.70
−75	4	0.87	0.83
−50	4	0.63	0.58
−25	5	0.80	0.74
0	5	0.69	0.52
25	6	0.91	0.80
50	6	0.91	0.79
75	6	1.01	0.93
100	5	0.86	0.81
125	4	0.80	0.78
150	6	0.82	0.74
175	5	0.84	0.80
200	7	0.86	0.77
225	7	0.93	0.86
250	6	0.91	0.81
275	7	0.83	0.75
300	4	0.60	0.58
325	5	0.85	0.80
350	5	0.89	0.83
375	5	0.92	0.85
400	6	0.74	0.66
425	5	0.76	0.70
450	6	0.71	0.62
475	7	0.86	0.75
500	7	0.78	0.59
525	6	1.11	1.00
550	7	1.09	0.90
575	7	0.88	0.77
600	6	0.48	0.38
625	6	0.62	0.53
650	4	0.44	0.39
675	5	0.63	0.55
700	4	0.59	0.50
725	4	0.78	0.70
750	4	0.62	0.59
775	4	0.69	0.66
800	5	0.58	0.50
825	4	0.74	0.72
850	4	0.71	0.68
875	4	0.83	0.78
900	5	0.75	0.66
925	4	0.58	0.54
950	5	0.57	0.52
975	5	0.69	0.63
1000	6	0.68	0.62
1025	3	0.72	0.70
1050	4	0.73	0.70
1075	4	0.82	0.78
1100	5	0.84	0.80
1125	4	0.88	0.85
1150	4	0.82	0.79
1175	5	0.81	0.77
1200	6	0.77	0.71
1225	5	0.94	0.87
1250	4	0.85	0.83
1275	4	1.01	0.98
1300	4	1.09	1.07
1325	5	1.20	1.15
1350	5	0.99	0.94
1375	6	0.98	0.90
1400	5	0.87	0.81
1425	4	1.03	0.97
1450	5	0.91	0.84
1475	6	1.02	0.96
1500	7	1.04	0.95
1525	5	1.18	1.03
1550	7	1.05	0.93
1575	3	1.00	0.96
1600	5	1.24	1.16
1625	5	1.54	1.45
1650	7	2.24	1.84
1675	8	2.14	1.61
1700	4	1.06	1.02
1725	6	1.02	0.94
1750	5	0.88	0.85
1775	4	1.14	1.11
1800	5	1.34	1.28
1825	5	1.36	1.31
1850	3	0.92	0.91
1875	5	1.44	1.38

[a] The window is denoted by the central time t_0.

[62] The spatial-temporal distribution of the input data, the uncertainty of the data and the technique used for modeling define the spatial and temporal resolution of the model. For the spatial resolution,

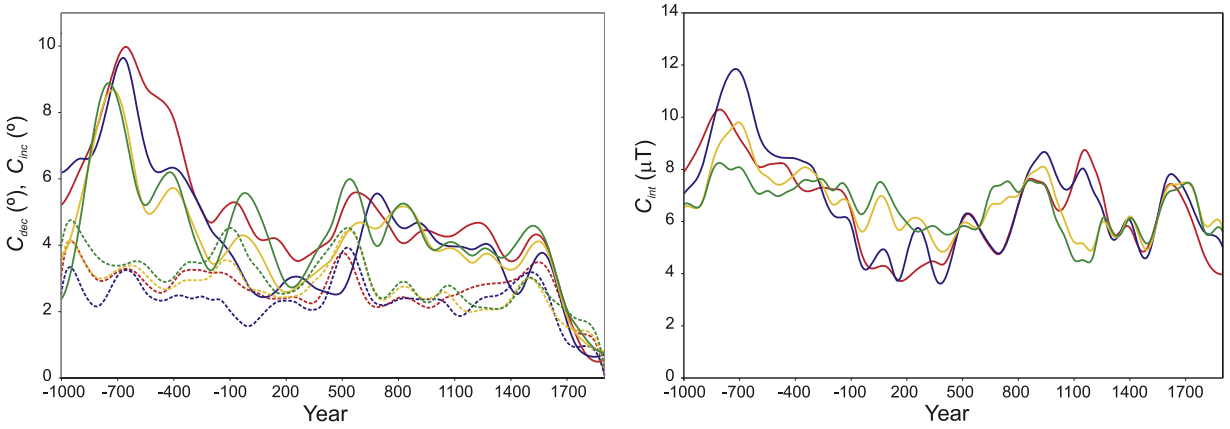

Figure 4. $C(t, \lambda, \varphi)$ error functions for (left) declination (C_{dec}, solid lines) and inclination (C_{inc}, dashed lines) and (right) intensity (C_{int}) components. This function has been calculated at different locations over Europe: north (red lines), 52°N latitude, 9°E longitude; west (blue lines), 44°N latitude, −4°W longitude; south (yellow lines), 40°N latitude, 12°E longitude; and east (green lines), 42°N latitude, 23°E longitude.

according to the model parameters (maximum degree and size of the cap), the model can reproduce wavelengths not lower than ∼5000 km [*Thébault et al.*, 2006]. Furthermore, the use of the sliding windows method with s = 50 years and 25 years overlapping between windows limits the temporal resolution to 75 years (3s/2).

[63] Figure 5 shows the declination, inclination and intensity maps for Europe and adjacent areas every 100 years from 1000 B.C. to 1900 A.D. Furthermore, an animation with declination, inclination and intensity maps is available as auxiliary material.[1]

[64] The obtained continuous geomagnetic field model for Europe and adjacent areas is available from the Web site: http://pc213fis.fis.ucm.es/scha.dif.3k_model.html. To generate a PSVC from SCHA.DIF.3K model it is only necessary to indicate the latitude and longitude of the site (input data). The output predictions are the declination, inclination and intensity (and their prediction uncertainties at 95% of confidence) versus time in ASCII format from 1000 B.C. to 1900 A.D.

5. Discussion: SCHA.DIF.3K Model and Input Data and Comparison With Global Models

[65] Values predicted by the model have been compared with the input data. The RMS misfit for data over the whole cap, averaged in 50 year bins, for declination, inclination and intensity are given in Figure 6. For comparison, we have added the spatial RMS misfit associated to the CALS7K.2 model [*Korte and Constable*, 2005] and the input models SCHA.DI.1-F and GUFM model (*Jackson et al.* [2000] modified according to *Gubbins et al.* [2006]).

[66] For the declination (Figure 6a) the RMS misfits of the regional model vary from 0.3° in 1875 ± 25 A.D. to 11.9° for 425 ± 25 B.C. The RMS error for CALS7K.2 model strongly increases between 1000 B.C. and 600 B.C. The distribution of the residual individual data has a Laplacian behavior with an average of −0.3° and a standard deviation of 4.0°. In Figure 6b, we have plotted the Laplace distribution curve (red curve) obtained with these statistical parameters. We have also calculated the cumulative distribution of the residual data and we have compared it with the theoretical Laplace cumulative distribution (Figure 6c). This comparison shows that the Laplace distribution is the suitable distribution for the actual residuals.

[67] The inclination RMS misfits are lower than the declination RMS misfits in absolute value (Figure 6d). For the regional model, the RMS error exhibits two maxima at 125 ± 25 B.C. (5.4°) and at 525 ± 25 A.D. (5.2°, which is bigger than the RMS errors from CALS7K.2), and two minima in 825 ± 25 B.C. (0.7°) and 1875 ± 25 A.D. (0.8°). The intensity errors (Figure 6g) show minima between 1025 and 1175 A.D. (∼ 4 μT) and maxima about 11.6 μT at 275 B.C. Figures 6e and 6h show the distribution of the individual data residuals for inclination and intensity, respectively. The Laplacian parameters for inclination and intensity residuals are −0.2°/0.1 μT (averaged residual) and 3.2°/7.5 μT (standard deviation). In this case,

[1]Auxiliary materials are available in the HTML. doi:10.1029/2008GC002244.

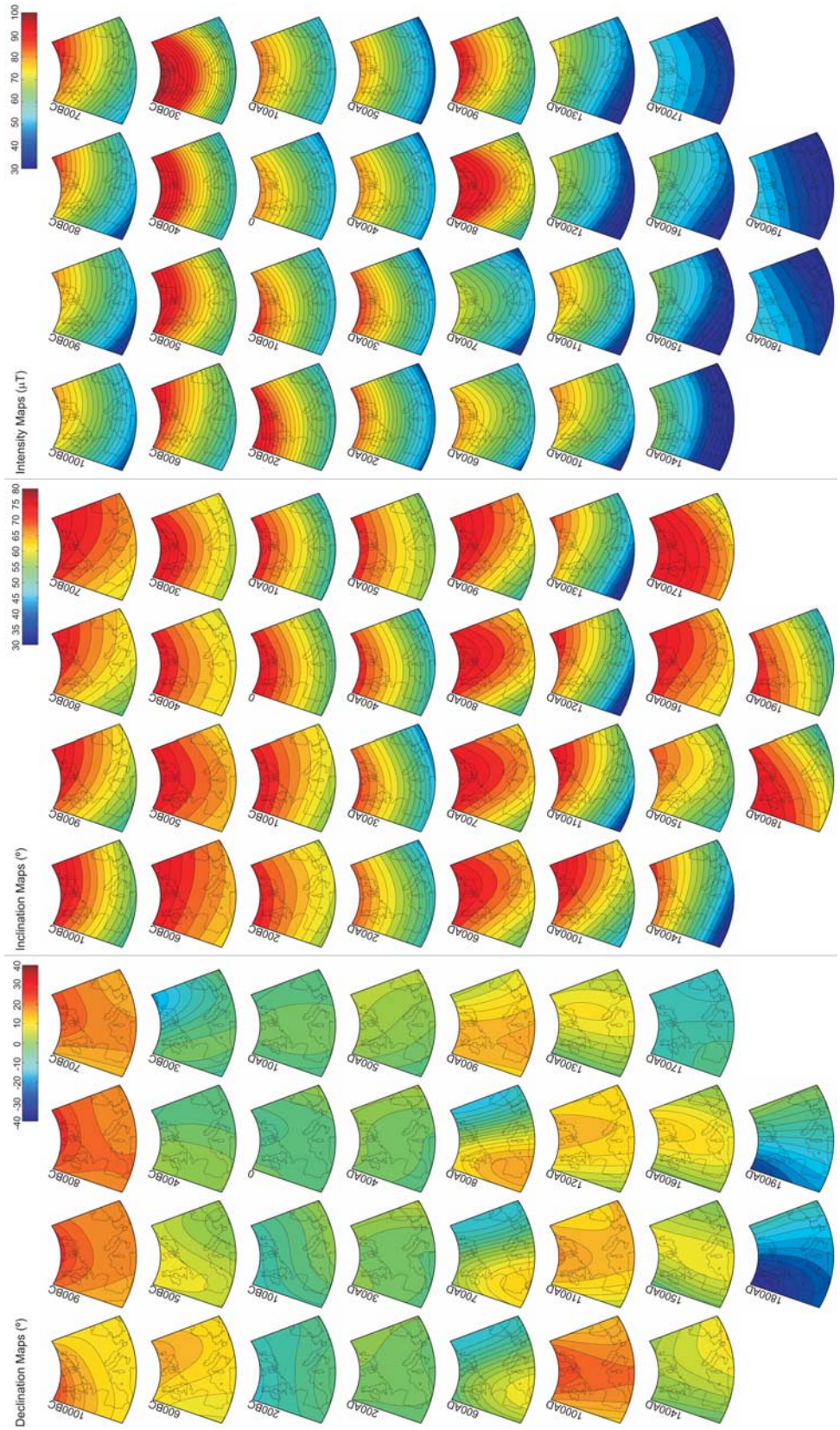

Figure 5. Snapshots from the SCHA.DIF.3K model for each 100 year interval. An animation is available as auxiliary material.

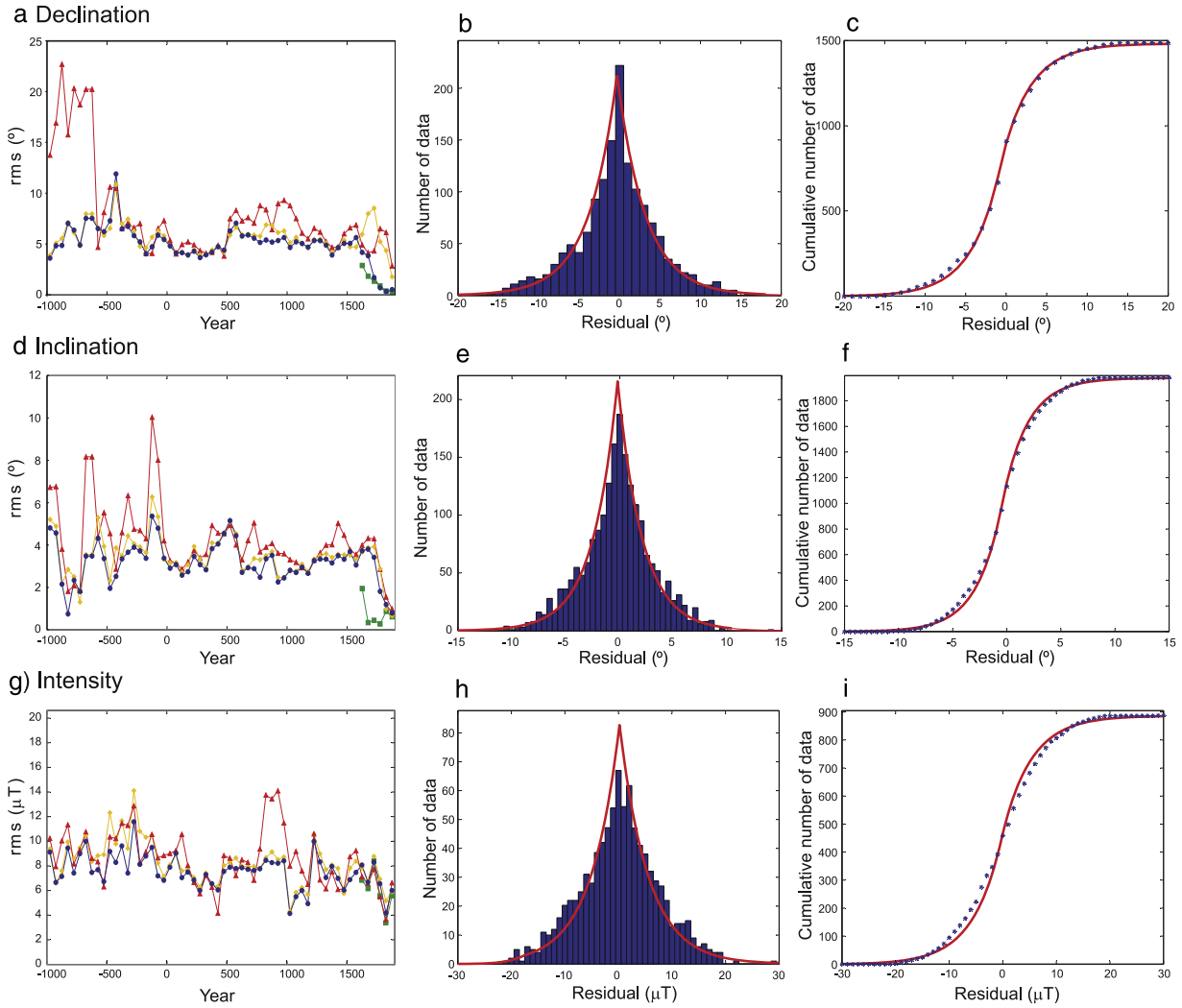

Figure 6. (a–c) Declination, (d–f) inclination, and (g–i) intensity RMS misfits (Figures 6a, 6d, and 6g), the residual distribution (Figures 6b, 6e, and 6h), and cumulative residual distribution (Figures 6c, 6f, and 6i). Figures 6a, 6d, and 6g show the RMS misfits (averaged for windows of 50 years) from the SCHA.DIF.3K model (blue line), from the CALS7K.2 (red line), from the SCHA.DI.1-F (yellow line), and from the GUFM model (green line). Figures 6b, 6e, and 6h show histograms of residual data; red lines are the Laplace distributions with the same mean and standard deviation. Figures 6c, 6f, and 6i show cumulative residual distribution (blue stars) and theoretical cumulative Laplace distributions (red lines).

the cumulative intensity residuals show a little difference with respect to the theoretical curve (Figure 6i) because of the high dispersion of this component. No major differences are observed between the RMS misfits associated with the regional and CALS7K.2 models for the inclination (except for the time interval 725 B.C. to 25 B.C.), but the RMS errors of the regional model are generally lower than the RMS errors of the CALS7K.2 global model for the intensity (especially between 700 A.D. and 1250 A.D.).

[68] We have compared the SCHA.DIF.3K model with the input models. The new regional model improved the previous model (SCHA.DI.1-F) for all the time interval (Figures 6a, 6d, and 6g). This improvement is clear for the declination after 1600 A.D. The RMS errors from the GUFM model are similar to the RMS errors from the regional model; an obvious result, since the global model is very similar to the regional one for the considered 1650–1900 period. Table 3 summarizes the averaged spatial-temporal RMS misfits for each element of the geomagnetic field and for the different models.

[69] To plot the SCHA.DIF.3K model with the input data, we have selected seven reference points to give predicted PSVC. These areas are shown in Figure 7. We have transferred both directional and

Table 3. Comparison of the Averaged Spatial-Temporal RMS Misfits Between SCHA.DIF.3K and Global Models CALS7K.2 and GUFM[a]

Models	RMS D (deg)	RMS I (deg)	RMS F (μT)
From 1000 B.C to 1900 A.D.			
SCHA.DIF.3K	2.4	2.3	7.6
CALS7K.2	5.3	3.3	8.8
From 1650 to 1900 A.D.			
SCHA.DIF.3K	1.2	1.4	6.3
GUFM[a]	1.2	1.1	6.4

[a] The GUFM model of *Jackson et al.* [2000] modified according to *Gubbins et al.* [2006].

intensity data from each site to the reference point by CVP and VADM methods respectively (VADM is the Virtual Axial Dipole Moment, i.e., an axial dipole field is assumed to transfer the intensity data to a reference point). The maximum distance between the site and the reference point was decided to be 700 km. Figure 8 shows the curves predicted by the regional model for each of the seven locations, along with their prediction uncertainty intervals at 95% of confidence. For comparison, we have also plotted the CALS7K.2 [*Korte and Constable*, 2005] and GUFM [*Jackson et al.*, 2000] global models and the input SCHA.DI.1-F model.

[70] Declination and inclination curves, i.e., directional curves show different behaviors in western Europe (Iberia, France, United Kingdom) and eastern Europe (Hungary, Bulgaria and Greece). The density of directional data is concentrated in the western area. The declination (Figure 8, left) in Europe shows several maximum peaks (easterly declinations), concentrated mainly in two time periods, around 800 B.C. and 1000–1100 A.D. The declination curves for the eastern side (Hungary and Bulgaria-Greece) show a significant maximum at 1575 A.D. For the Roman period, the declination has low values and little variation (see also Figure 5, from 100 B.C. to 400 A.D.). The minima declination values (westerly declinations) are achieved at 400 B.C., 600 A.D. and at recent times, around the 18th century.

[71] The global model CALS7K.2 shows a similar variation to declination as the regional model, but underfitting all peaks because of the strong smoothing of the model. This smoothing is clearly visible for the period 1000 B.C. to 500 B.C., where the global model gives declination values close to zero, while the regional model records its highest maximum of declination (between 23° and 25° for the whole European area). The biggest differences between global and regional models are recorded during this time period; however, it is worth remembering that input data from this epoch are extremely scarce (CALS7K.2 model used lake sediments data for this epoch).

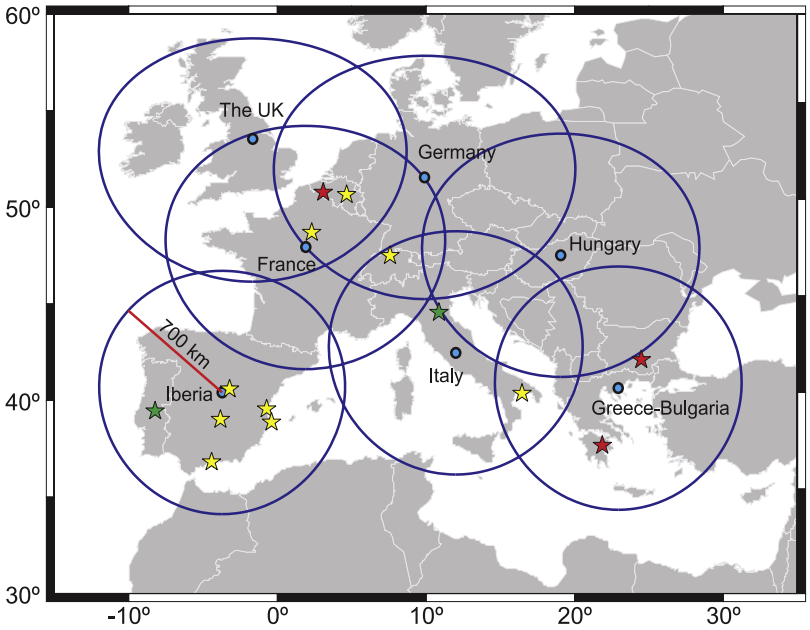

Figure 7. Considered areas (blue circles) to compare the SCHA.DIF.3K model to the input data. Blue points are the reference site (see text for details). Locations of archeomagnetic dating studies with all geomagnetic components (D, I, and F, red stars) and directional components (D and I, green stars). Location of the new intensity data (yellow stars).

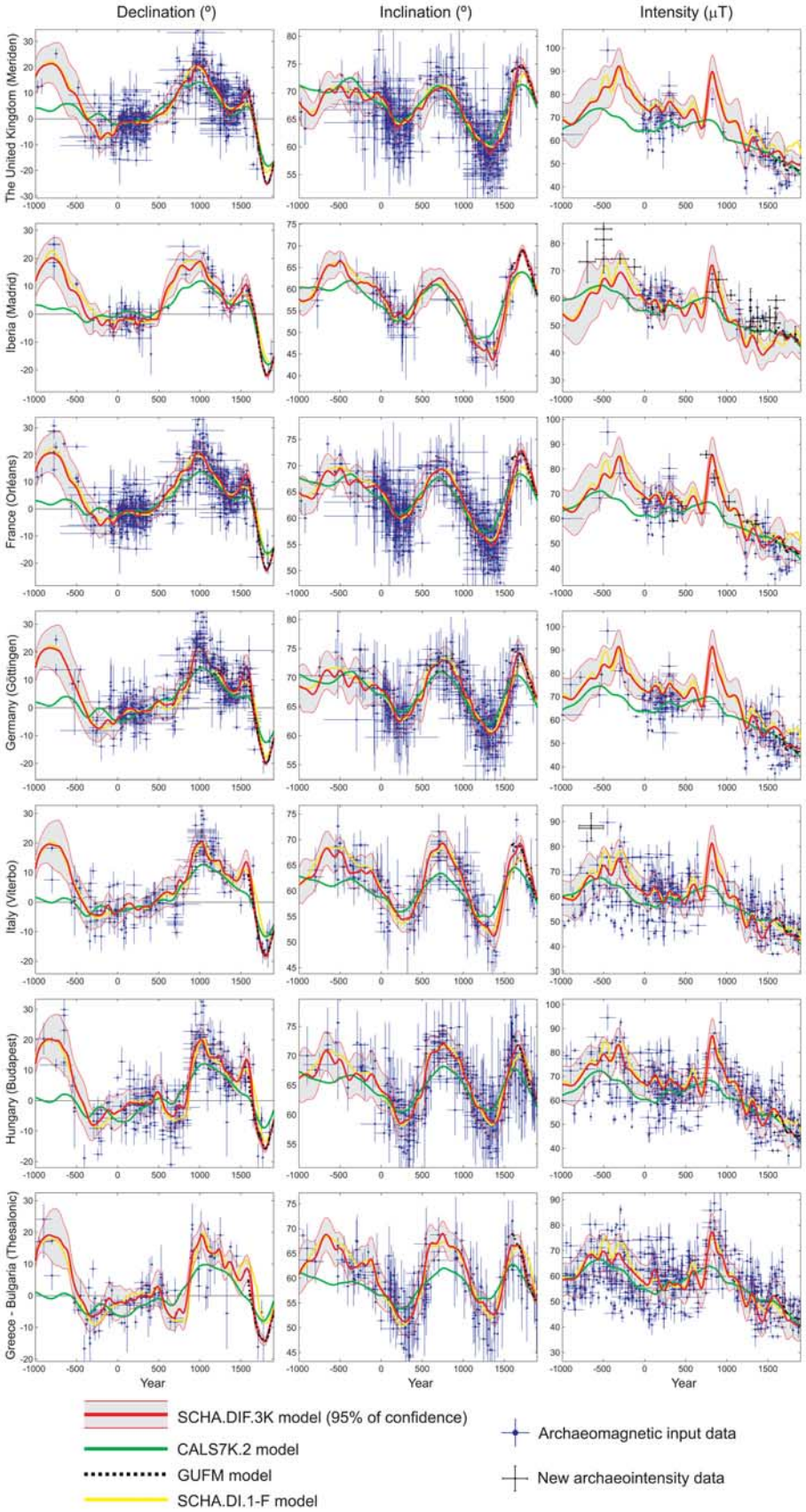
Declination (º)
Inclination (º)
Intensity (μT)
The United Kingdom (Meriden)
Iberia (Madrid)
France (Orléans)
Germany (Göttingen)
Italy (Viterbo)
Hungary (Budapest)
Greece - Bulgaria (Thesalonic)
Year
SCHA.DIF.3K model (95% of confidence)
CALS7K.2 model
GUFM model
SCHA.DI.1-F model
Archaeomagnetic input data
New archaeointensity data

Figure 8

[72] The inclination curves (Figure 8, middle) show a sinusoidal appearance with maximums peaks at 500 B.C., 750 A.D. and 1700 A.D. The most relevant minimum peaks are found around 320 A.D. and 1325 A.D. This behavior is also reflected in the CALS7K.2 global model, but the predicted curves again show underfitting for these peaks (especially for Italy, Hungary and Greece-Bulgaria). The greatest discrepancy between the regional and global models occurs again during the years B.C.

[73] The density of intensity values (Figure 8, right) is higher in eastern Europe (Hungary, Bulgaria and Greece) than in western Europe, where data are mainly divided into two time periods: 0–400 A.D. and 1250–1800 A.D. This could indicate an underfitting of intensity data in western Europe. To evaluate this problem, we have considered intensity data from western European countries not included in the regional model (yellow stars in Figure 7). These data come from recent publications [*Nachasova et al.*, 2007, and references therein; *Gómez-Paccard et al.*, 2008] and from archeointensity studies product of the European AARCH project [*Batt et al.*, 2008, and references therein]. These new intensity data have been plotted in Figure 8 reduced by VADM to the nearby reference point. As shown in Figure 8, the predictions by the regional model are in agreement with the new intensity data, especially in the maxima around 500–300 B.C. and ~ 800 A.D. Therefore, we think that the model predicts the intensity over Europe in a proper manner. The intensity curves generated by the SCHA.DIF.3K model have a common behavior throughout Europe.

[74] The regional model suggests that the Earth's magnetic field strength reached 10 maxima in Europe at 600–500 and 275 B.C., and at 160, 325, 580, 820, 1310, 1550–1700 and 1780 A.D. On the other hand, the CALS7K.2 global model [*Korte and Constable*, 2005] is too smoothed to describe fluctuations shown by the data at these locations. This global model exhibits only two maxima, around 500 B.C. and 800 A.D.

[75] The comparison between the new regional model and the input models (Figure 8) shows that the difference is due to the data density and their temporal distribution. The new model is close to the input models when the data density is low, which is logical. Before 200 B.C., both new and input models are very similar for the three components in western Europe, again in agreement with the low data density there (Figure 2c). However, for this time interval, differences are found in the inclination and intensity curves from eastern Europe, where the density of inclination and intensity data is higher (Figures 2b and 2c). The new regional model agrees with the GUFM model modified according to *Gubbins et al.* [2006].

6. Applications

6.1. Archeomagnetic Dating

[76] One of the immediate applications of SCHA.DIF.3K regional model is its use as tool for archeomagnetic dating. So far the PSVC determined for a region have been used for archeomagnetic dating. The limitation of this application is the distance from the dating point to the location of the reference curve (the relocation error). In addition it must be borne in mind that the PSVC are individually generated for each region, so there is no consistency enforced between curves from neighboring areas.

[77] The use of the SCHA.DIF.3K model as a tool for archeomagnetic dating represents an improvement for several reasons. First of all, the regional model has been generated considering all elements of the geomagnetic field (declination, inclination and intensity). Second, the regional model is built with an in situ archeomagnetic database. Furthermore, the database covers the whole time period from 1000 B.C. to 1900 A.D., while the database used in the PSVC has gaps of data for any time interval. Finally, and more important, we can generate a PSVC at the location of the archeological structure, avoiding in this way the relocation error associated with traditional PSVC.

[78] To demonstrate the utility of the regional SCHA.DIF.3K model, we have used it to date five archeological structures which have also been dated by the classical archeomagnetic method [*Lanos*, 2004]. Therefore the studied selected sites are located close to the available Bayesian reference PSVC. Archeological evidence has estab-

Figure 8. (left) Declination, (middle) inclination, and (right) intensity data (blue points with uncertainty bars) and model predictions (solid red line) with the prediction uncertainty (gray shading) for the last 3000 years. The CALS7K.2 (green line) and the input models SCHA.DI.1-F (yellow line) and GUFM (green line) have been plotted. New intensity values (black points with error bars) have been plotted in different intensity curves (see text for details).

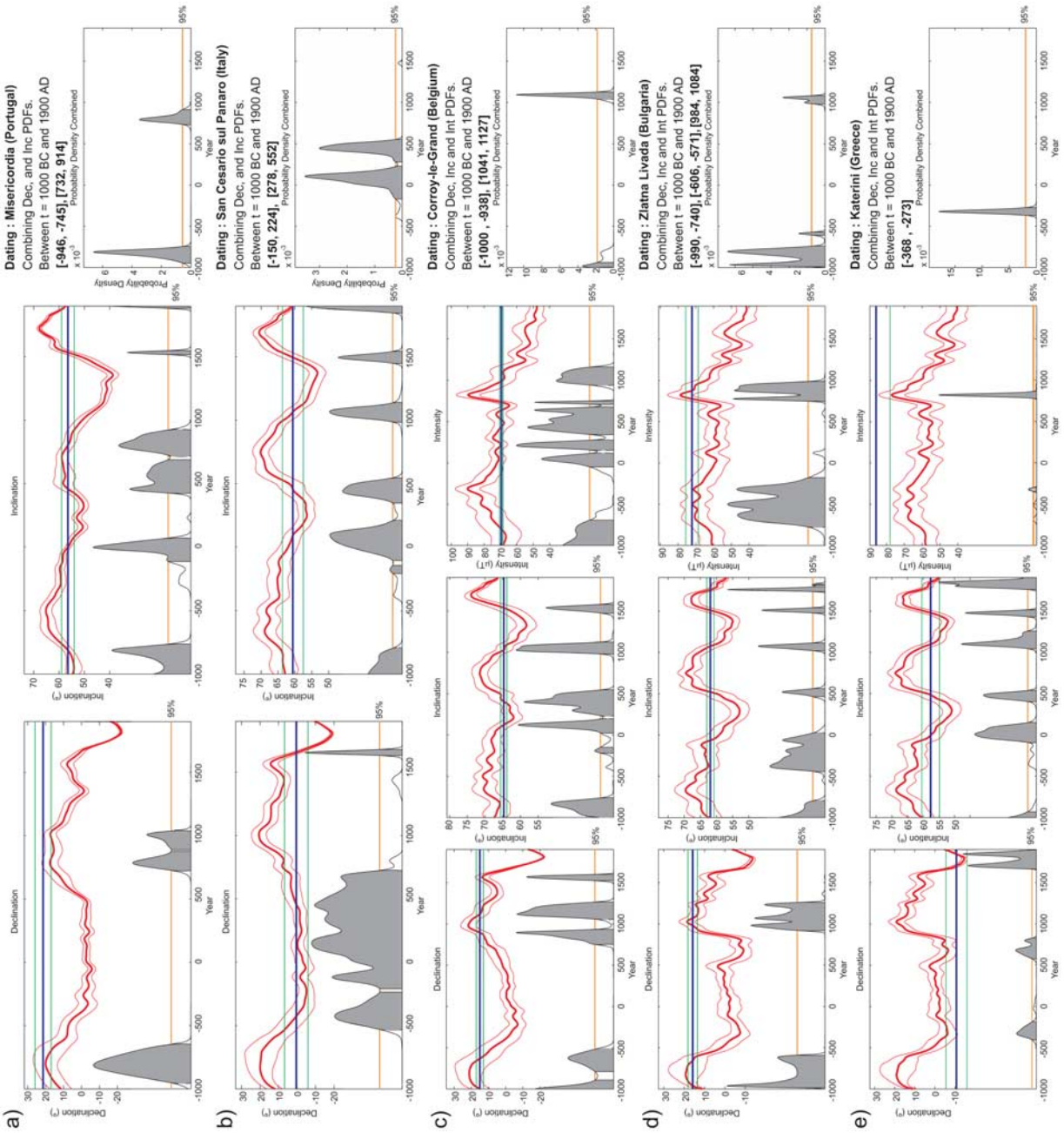
a)
Dating : Misericordia (Portugal)
Combining Dec, and Inc PDFs.
Between t = 1000 BC and 1900 AD
[-946, -745], [732, 914]
b)
Dating : San Cesario sul Panaro (Italy)
Combining Dec, and Inc PDFs.
Between t = 1000 BC and 1900 AD
[-150, 224], [278, 552]
c)
Dating : Corroy-le-Grand (Belgium)
Combining Dec, Inc and Int PDFs.
Between t = 1000 BC and 1900 AD
[-1000 , -938], [1041, 1127]
d)
Dating : Zlatna Livada (Bulgaria)
Combining Dec, Inc and Int PDFs.
Between t = 1000 BC and 1900 AD
[-990, -740], [-606, -571], [984, 1084]
e)
Dating : Katerini (Greece)
Combining Dec, Inc and Int PDFs.
Between t = 1000 BC and 1900 AD
[-368 , -273]
Probability Density Combined
Declination
Inclination
Intensity
Year
95%

Figure 9

Table 4. Archeomagnetic Dating by SCHA.DIF.3K Model[a]

Site	Archeological Estimation	Archeomagnetic Dating by PSVC	Archeomagnetic Dating by SCHA.DIF.3K Model
Misericordia (Portugal)	Late Bronze Age, first half of C9 B.C. until C8 B.C.	[−834, −709]	[−946, −745]
San Cesario sul Panaro (Italy)	From C3 to C4 A.D.	[−99, 650]	[−150, 224] * [278, 552]
Corroy-le-Grand (Belgium)	Second half of C10 until C12 A.D.	[1022, 1167]	[1041, 1127]
Zlatna Livada (Bulgaria)	C11–C12 A.D.	[826, 1004]	[984, 1084]
Katerini (Greece)	Late C4 B.C. to early C2 B.C.	[−505, −287]	[−368, −273]

[a] See text for details.

lished the age of each structure (age of the last usage). Archeomagnetic data (declination, inclination and/or intensity) from these structures have not been included in the generation of the regional model, so they constitute an independent set of data. The studied structures correspond to five European sites: Misericordia (Serpa, Portugal [*Catanzariti et al.*, 2008]); San Cesario sul Panaro (Bazzano, Italy [*Tema and Lanza*, 2008]); Corroy-le-Grand (Belgium [*Spassov et al.*, 2008]); Katerini (Greece [*De Marco et al.*, 2008]) and Zlatna Livada (Bulgaria [*Herries et al.*, 2008]). Two of the five sites (Misericordia and San Cesario sul Panaro) have only directional data (declination and inclination). The location of each structure is shown in Figure 7.

[79] The archeomagnetic dating has been carried out according to the mathematical method of *Lanos* [2004], where archeomagnetic data are compared with a PSVC. In our case, the PSVC is generated by the regional SCHA.DIF.3K model avoiding the relocation error. So, we can obtain the probability density functions (PDF) for each data (D, I and/or F), whose combination generates the final PDF (combined PDF). The combined PDF is used to define the dating period time at 95% of confidence.

[80] Figure 9 shows the five archeomagnetic datings along with the PDF of each archeomagnetic element and the combined PDF, with the determined confidence intervals at 95% of probability. Table 4 summarizes these time intervals, the archeological information and time intervals obtained from the archeomagnetic dating with PSVC close to the sampling site. The structures used for this application are located close to the published Bayesian PSVC, therefore the relocation error should be small and both archeomagnetic methods should produce similar results. For all cases there is a good agreement between the archeomagnetic dating by SCHA.DIF.3K model, by the PSVC, and by the archeological information.

[81] This new method can also be applied in other European regions where reference PSVC are not available.

6.2. Archeomagnetic Jerks

[82] Archeointensity data from Europe covering the last three millennia show coincidence between sharp changes in the direction of the geomagnetic field with intensity maxima during short periods of less than 1 century: archeomagnetic jerks (AMJ) according to *Gallet et al.* [2003, 2005] with a time scale between geomagnetic jerks (years) and excursions (thousands of years). *Gallet et al.* [2005] analyzed the intensity data from western Europe and the eastern Mediterranean. They detected 4 AMJ for the last three millennia, around 800 B.C., 200 A.D., 750 A.D., and 1400 A.D. However, the evidence for these jerks is limited, given the density of data used by *Gallet et al.* [2003, 2005]. *Snowball and Sandgren* [2004] concluded, from high resolution sedimentary data, that significant century scale increases and decreases in relative field intensity between 4000 and 2000 cal B.P.

Figure 9. Archeomagnetic dating. The PSVC from SCHA.DIF.3K model (red curve) at each location and the archeomagnetic data (blue line). Their uncertainty envelopes are shown in red and green, respectively. The probability density functions (a and b) for declination and inclination and (c–e) for intensity and combined declination-inclination (Figures 9a and 9b) and declination-inclination-intensity (Figures 9c–9e) are shaded at the 95% (orange line in probability density functions). The most probable age for every site is shown in brackets.

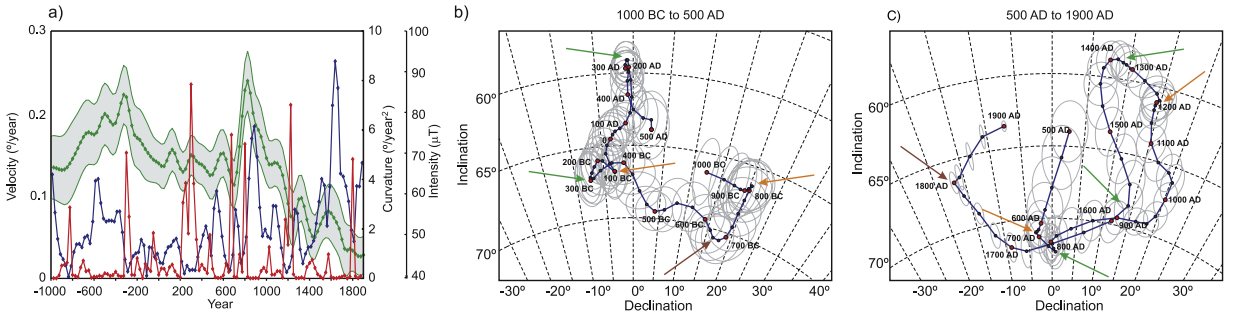

Figure 10. Archeomagnetic jerks: (a) Velocity (blue line) and curvature for the directional curve (red line) and intensity curve (green line) with the prediction uncertainty band (gray band) at the center of Europe (48°N, 9°E). Directional curve plotted in an equal area diagram (b) from 1000 B.C. to 500 A.D. and (c) from 500 A.D. to 1900 A.D. with the prediction uncertainty (gray ellipses). Red circles are marked every 100 years. Green arrows indicate proposed jerks according to *Gallet et al.* [2003, 2005] (coincidence between sharp changes in the direction of the geomagnetic field with intensity maxima). Orange arrows indicate abrupt changes in the direction (small or no intensity maxima). Brown arrows indicate possible jerks.

were associated with abrupt changes (jerks) in the direction of the geomagnetic vector.

[83] The regional SCHA.DIF.3K allows for the study of potential AMJ by analyzing the intensity maxima, the magnitude of directional velocity, or angular rate of change of direction and the maximum curvature of the archeomagnetic curve. We have calculated the velocity and curvature of the directional curve at the center of the cap (48°N of latitude and 9°E of longitude). Results are shown in Figure 10, along with the intensity curve for this location.

[84] We can see 5 epochs where a maximum in intensity coincides with a maximum of curvature and a minimum in velocity (Figure 10) around 300 B.C., and 300, 800, 1350, and 1600 A.D. And a less well defined event could also have occurred around 1800 A.D. (small intensity maxima). Another event characterized by a directional change together with a small intensity maxima occurred around 650 B.C.; and rapid directional changes associated with velocity minima (but no intensity maxima) took place around 825 B.C., 125 B.C., 650 A.D. and 1200 A.D.

[85] According to *Gallet et al.*'s [2003, 2005] definition of AMJ, we can propose five clear AMJ around 275–325 B.C. (AMJ-300), 275–325 A.D. (AMJ300), 775–825 A.D. (AMJ800), 1350 A.D. (AMJ1350) and 1550–1600 A.D. (AMJ1600) and a suspected jerk at 1775–1800 A.D. (AMJ1800).

[86] It is important to point out that the AMJ1350 is best defined in western Europe, while the AMJ1600 is evidenced from eastern Europe studies. This is due to the inhomogeneous distribution of data in Europe already mentioned. More archeomagnetic information, well distributed in Europe and well dated, is necessary in both periods to better define these events. Similarly, an additional possible AMJ is suspected around 650–700 B.C. (AMJ-650), but it needs to be confirmed with more data. During the period 600–900 A.D. two AMJ could have occurred instead of the only one that we propose here, but during the "dark ages" the number of archeomagnetic data is small and the confidence in dating is low.

[87] The AMJ proposed by *Gallet et al.* [2005] around 800 B.C. correspond to an abrupt directional change (maximum curvature and minimum velocity), but no global intensity maximum is observed. It has to be noted that *Gallet et al.* [2005] only had a single intensity datum for that epoch. More studies are necessary to investigate this event. Other abrupt directional changes are observed around 125 B.C. and 1200 A.D.

7. Conclusions

[88] We have developed a new regional archeomagnetic model for Europe for the last 3000 years. The model has been calculated by using the SCHA regional technique, modified for modeling the three elements of the geomagnetic field together: declination, inclination and intensity. The SCHA.DIF.3K model allows a complete description of the geomagnetic field over Europe and adjacent areas for the last 3000 years, and suggests that the Earth's magnetic field has experienced a minimum of 5 archeomagnetic jerks in Europe for the last 3000 years (AMJ-300, AMJ300, AMJ800, AMJ1350, AMJ1600) and a suspected jerk (AMJ1800). These events are

characterized by intensity maxima, velocity minima and a sharp change in curvature. Other events are observed around 825 B.C., 650–700 B.C., 125 B.C., 600–650 A.D. and 1175–1200 A.D. which seem ''directional jerks,'' but need to be confirmed with more data. We have also demonstrated that the regional model is an appropriate tool for archeomagnetic dating, since a PSVC can be generated at the location of the archeological structure, thus avoiding the traditional relocation error. The model fits the present archeomagnetic database for Europe more accurately than the global model proposed by *Korte and Constable* [2005] for the 1000 B.C. to 1900 A.D. time interval. The discrepancies with CALS7K.2 reflect the difference in the data sets used and uncertainties assigned, the choice of least sums of absolute deviation versus regularized inversion in the spatial domain, and the use of sliding windows versus continuous time variations.

Acknowledgments

[89] The authors are grateful to the Spanish research projects CGL2005-00211 and CGL2008-02203/BTE and the FPI grant BES-2006-13488. Constructive comments and suggestions from Catherine Constable, Monika Korte, and a third anonymous reviewer have highly improved the manuscript and are therefore gratefully acknowledged. All algorithms have been developed in Matlab® codec (Matlab 7.0.4, R14) along with the figures and animations.

References

Alexandrescu, M., V. Courtillot, and J.-L. Le Mouël (1996), Geomagnetic field direction in Paris since the mid-sixteenth century, *Phys. Earth Planet. Inter.*, *98*, 321–360, doi:10.1016/S0031-9201(96)03194-9.

Batt, C. M., I. Zananiri, and D. H. Tarling (2008), Preface: Archaeomagnetic applications for the rescue of cultural heritage, *Phys. Chem. Earth*, *33*, 403–406, doi:10.1016/j.pce.2008.02.015.

Cafarella, L., A. De Santis, and A. Meloni (1992), *The Historical Italian Geomagnetic Data Catalogue*, 160 pp., Ist. Naz. di Geofis. e Vulcanol., Rome.

Casas, L., and A. Incoronato (2007), Distribution analysis of errors due to relocation of geomagnetic data using the 'Conversion via Pole' (CVP) method: Implications on archaeomagnetic data, *Geophys. J. Int.*, *169*(2), 448–454, doi:10.1111/j.1365-246X.2007.03346.x.

Catanzariti, G., G. McIntosh, A. M. Monge Soares, E. Díaz-Martínez, P. Kresten, and M. L. Osete (2008), Archaeomagnetic dating of a vitrified wall at the Late Bronze Age settlement of Misericordia (Serpa, Portugal), *J. Archaeol. Sci.*, *35*, 1399–1407.

Chauvin, A., Y. Garcia, P. Lanos, and F. Laubenheimer (2000), Paleointensity of the geomagnetic field recovered on archaeomagnetic sites from France, *Phys. Earth Planet. Inter.*, *120*, 111–136, doi:10.1016/S0031-9201(00)00148-5.

De Marco, E., S. Spassov, D. Kondopoulou, I. Zananiri, and E. Gerofoka (2008), Arcaheomagnetic study and dating of a Hellenistic site in Katerini (N. Greece), *Phys. Chem. Earth*, *33*, 481–495.

De Santis, A., D. J. Kerridge, and D. R. Barraclough (1989), A spherical cap harmonic model of the crustal magnetic anomaly field in Europe by Magsat, in *Geomagnetism and Paleomagnetism*, edited by F. J. Lowes et al., pp. 1–17, Kluwer, Dordrecht, Netherlands.

Evans, M. E. (2006), Archaeomagnetic investigations in Greece and their bearing on geomagnetic secular variation, *Phys. Earth Planet. Inter.*, *159*, 90–95, doi:10.1016/j.pepi.2006.06.005.

Evans, M. E., and G. S. Hoye (2005), Archaeomagnetic results from southern Italy and their bearing on geomagnetic secular variation, *Phys. Earth Planet. Inter.*, *151*, 155–162.

Gallet, Y., A. Genevey, and M. Le Goff (2002), Three millennia of directional variations of the Earth's magnetic field in western Europe as revealed by archaeological artefacts, *Phys. Earth Planet. Inter.*, *131*, 81–89, doi:10.1016/S0031-9201(02)00030-4.

Gallet, Y., A. Genevey, and V. Courtillot (2003), On the possible occurrence of archeomagnetic jerks in the geomagnetic field over the past three millennia, *Earth Planet. Sci. Lett.*, *214*, 237–242, doi:10.1016/S0012-821X(03)00362-5.

Gallet, Y., A. Genevey, and F. Fluteau (2005), Does Earth's magnetic field secular variation control centennial climate change?, *Earth Planet. Sci. Lett.*, *236*, 339–347, doi:10.1016/j.epsl.2005.04.045.

Gómez-Paccard, M., et al. (2006a), A catalogue of Spanish archaeomagnetic data, *Geophys. J. Int.*, *166*, 1125–1143, doi:10.1111/j.1365-246X.2006.03020.x.

Gómez-Paccard, M., P. Lanos, A. Chauvin, G. McInstosh, M. L. Osete, G. Catanzariti, V. C. Ruiz-Martínez, and J. I. Núñez (2006b), First archaeomagnetic secular variation curve for the Iberian Peninsula: Comparison with other data from western Europe and with global geomagnetic field models, *Geochem. Geophys. Geosyst.*, *7*, Q12001, doi:10.1029/2006GC001476.

Gómez-Paccard, M., A. Chauvin, P. Lanos, J. Thiriot, and P. Jiménez-Castillo (2006c), Archeomagnetic study of seven contemporaneous kilns from Murcia (Spain), *Phys. Earth Planet. Inter.*, *157*, 16–32, doi:10.1016/j.pepi.2006.03.001.

Gómez-Paccard, M., A. Chauvin, P. Lanos, and J. Thiriot (2008), New archeointensity data from Spain and the geomagnetic dipole moment in western Europe over the past 2000 years, *J. Geophys. Res.*, *113*, B09103, doi:10.1029/2008JB005582.

Gubbins, D., A. L. Jones, and C. C. Finlay (2006), Fall in Earth's magnetic field is erratic, *Science*, *312*(5775), 900–902, doi:10.1126/science.1124855.

Haines, G. V. (1985), Spherical cap harmonic analysis, *J. Geophys. Res.*, *90*(B3), 2583–2591, doi:10.1029/JB090iB03p02583.

Haines, G. V. (1988), Computer programs for spherical cap harmonic analysis of potential and general fields, *Comput. Geosci.*, *14*(4), 413–447, doi:10.1016/0098-3004(88)90027-1.

Herries, A. I. R., M. Kovacheva, and M. Kostadinova (2008), Mineral magnetism and archaeomagntic dating of a mediaeval oven from Zlatna Livada, Bulgaria, *Phys. Chem. Earth*, *33*, 496–510.

Hongre, L., G. Hulot, and A. Khokhlov (1998), An analysis of the geomagnetic field over the past 2000 years, *Phys. Earth Planet. Inter.*, *106*, 311–335, doi:10.1016/S0031-9201(97)00115-5.

Jackson, A., A. R. T. Jonkers, and M. R. Walker (2000), Four centuries of geomagnetic secular variation from historical

records, *Philos. Trans. R. Soc. London, Ser. A*, *358*, 957–990, doi:10.1098/rsta.2000.0569.

Jonkers, A. R. T., A. Jackson, and A. Murray (2003), Four centuries of geomagnetic data from historical records, *Rev. Geophys.*, *41*(2), 1006, doi:10.1029/2002RG000115.

Korte, M., and C. G. Constable (2003), Continuous global geomagnetic field models for the past 3000 years, *Phys. Earth Planet. Inter.*, *140*, 73–89, doi:10.1016/j.pepi.2003.07.013.

Korte, M., and C. G. Constable (2005), Continuous geomagnetic field models for the past 7 millennia: 2. CALS7K, *Geochem. Geophys. Geosyst.*, *6*, Q02H16, doi:10.1029/2004GC000801.

Korte, M., A. Genevey, C. G. Constable, U. Frank, and E. Schnepp (2005), Continuous geomagnetic field models for the past 7 millennia: 1. A new global data compilation, *Geochem. Geophys. Geosyst.*, *6*, Q02H15, doi:10.1029/2004GC000800.

Lanos, P. (2004), Bayesian inference of calibration curves: Application to archaeomagnetism, in *Tools for Constructing Chronologies: Crossing Disciplinary Boundaries*, vol. 177, edited by C. Buck and A. Millard, pp. 43–82, Springer, London.

Lodge, A., and R. Holme (2009), Towards a new approach to archaeomagnetic dating in Europe using geomagnetic field modelling, *Archaeometry*, doi:10.1111/j.1475-4754.2008.00400.x, in press.

Malin, S. R. C., and E. C. Bullard (1981), The direction of the Earth's magnetic field at London, 1570–1975, *Philos. Trans. R. Soc. London, Ser. A*, *299*, 357–423, doi:10.1098/rsta.1981.0026.

Márton, P., and E. Ferencz (2006), Hierarchical versus stratification statistical analysis of archaeomagnetic directions: The secular variation curve for Hungary, *Geophys. J. Int.*, *164*, 484–489, doi:10.1111/j.1365-246X.2006.02873.x.

Nachasova, I. E., K. S. Burakov, and A. J. Lorrio (2007), Archaeomagnetic study of ceramics from the El Molon Archaeological Monument (Spain), *Izv. Phys. Solid Earth*, *43*(10), 830–835.

Noël, M., and C. M. Batt (1990), A method for correcting geographically separated remanence directions for the purpose of archaeomagnetic dating, *Geophys. J. Int.*, *102*, 753–756, doi:10.1111/j.1365-246X.1990.tb04594.x.

Pavón-Carrasco, F. J., M. L. Osete, J. M. Torta, L. R. Gaya-Piqué, and P. Lanos (2008a), Initial SCHA.DI.00 regional archaeomagnetic model for Europe for the last 2000 years, *Phys. Chem. Earth*, *33*(6–7), 596–608.

Pavón-Carrasco, F. J., M. L. Osete, J. M. Torta, and L. R. Gaya-Piqué (2008b), A regional archaeomagnetic model for the palaeointensity in Europe for the last 2000 years and its implications for climatic change, *Pure Appl. Geophys.*, *165*(6), 1209–1225, doi:10.1007/s00024-008-0354-4.

Ruíz-Martínez, V. C., F. J. Pavón-Carrasco, and G. Catanzariti (2008), First archaeomagnetic data from northern Iberia, *Phys. Chem. Earth*, *33*, 566–577.

Schnepp, E., and P. Lanos (2005), Archaeomagnetic secular variation in Germany during the past 2500 years, *Geophys. J. Int.*, *163*, 479–490, doi:10.1111/j.1365-246X.2005.02734.x.

Schnepp, E., and P. Lanos (2006), A preliminary secular variation reference curve for archaeomagnetic dating in Austria, *Geophys. J. Int.*, *166*(1), 91–96, doi:10.1111/j.1365-246X.2006.03012.x.

Snowball, I., and P. Sandgren (2004), Geomagnetic field intensity changes in Sweden between 9000 and 450 cal BP: Extending the record of "archaeomagnetic jerks" by means of lake sediments and the pseudo-Thellier technique, *Earth Planet. Sci. Lett.*, *227*, 361–376, doi:10.1016/j.epsl.2004.09.017.

Spassov, S., J. Hus, R. Geeranerts, and F. Heller (2008), Archaeomagnetic dating of a High Middle Age likely iron working site in Corroy-le-Grand (Belgium), *Phys. Chem. Earth*, *33*, 544–556.

Tema, E., and R. Lanza (2008), Archaeomagnetic study of a lime kiln at Bazzano (northern Italy), *Phys. Chem. Earth*, *33*, 534–543.

Tema, E., I. Hedley, and P. Lanos (2006), Archaeomagnetism in Italy: A compilation of data including new results and a preliminary Italian secular variation curve, *Geophys. J. Int.*, *167*, 1160–1171, doi:10.1111/j.1365-246X.2006.03150.x.

Thébault, E. (2008), A proposal for regional modelling at the Earth's surface, R-SCHA2D, *Geophys. J. Int.*, *174*, 118–134, doi:10.1111/j.1365-246X.2008.03823.x.

Thébault, E., J. J. Schott, and M. Mandea (2006), Revised spherical cap harmonic analysis (R-SCHA): Validation and properties, *J. Geophys. Res.*, *111*, B01102, doi:10.1029/2005JB003836.

Torta, J. M., L. R. Gaya-Piqué, and A. De Santis (2006), Spherical cap harmonic analysis of the geomagnetic field with application for aeronautical mapping, in *Geomagnetics for Aeronautical Safety: A Case Study in and Around the Balkans*, edited by J. L. Rasson and T. Delipetrov, pp. 291–307, Springer, Dordrecht, Netherlands.

Zananiri, I., C. M. Batt, P. Lanos, D. H. Tarling, and P. Linford (2007), Archaeomagnetic secular variation in the UK during the past 4000 years and its application to archaeomagnetic dating, *Phys. Earth Planet. Inter.*, *160*(2), 97–107.